Int. J. Heat Mass Transfer. Vol. 14, pp. 2063–2082. Pergamon Press 1971. Printed in Great Britain

TURBULENT FLOW OF GAS MIXTURES UNDERGOING EQUILIBRIUM AND NONEQUILIBRIUM REACTIONS IN A TUBE WITH SURFACE MASS TRANSFER*

Y. C. WU†, A. F. MILLS and V. E. DENNY
University of California, Los Angeles, California 90024, U.S.A.

(*Received* 4 *December* 1970 *and in revised form* 17 *March* 1971)

Abstract—A finite difference method has been developed for the solution of turbulent tube flows of effectively binary, ideal gas mixtures undergoing equilibrium or nonequilibrium chemical reactions, and with mass injection at the tube wall. Axial diffusion of mass species, momentum and thermal energy are neglected in order to yield parabolic governing conservation equations. The van Driest formulation for the eddy diffusivity has been extended to include the effects of variable properties and surface mass transfer. Computational procedures have been developed for incorporating the eddy diffusivity model into turbulent flow calculations for both internal and external boundary layer flows.

The overall numerical method has been applied to flows of non-reacting air, equilibrium mixtures of N_2O_4 and NO_2, and nonequilibrium mixtures of NO_2, NO and O_2, with O_2 injection through the tube wall. Results are reported here for pressure drop, skin friction coefficient; surface heat flux and species mass transfer conductances; the agreement with available experimental data is satisfactory. The present method is demonstrated to be a significant advance over methods previously used to analyze chemically reacting turbulent tube flows.

NOMENCLATURE

c, molar concentration;
C_f, skin friction coefficient;
C_p, C_{pi}, constant pressure specific heats for the mixture, species i;
D, tube diameter;
$\mathscr{D}$, average binary diffusion coefficient;
$G(y_i^+)$, factor defined in equation (19);
h, h_i, specific enthalpy of mixture, species i;
j, diffusive mass flux;
K, universal constant in mixing length theory;
K^+, universal constant carrying the damping factor defined by equation (16);
$K_p^{(r)}$, equilibrium constants defined by equations (20) and (21);
$k_f^{(r)}$, forward reaction rate constant for the r'th reaction;
M, M_i, molecular weight of mixture, species i;
m_i, mass fraction;
$\dot{m}$, surface mass transfer rate $= (\rho v)_s$;
p, pressure;
Pr_e, effective Prandtl number, defined by equation (8);
q, conductive heat flux;
R, R^+, tube radius, $u_{\tau_s}R/\nu$;
$\mathscr{R}$, universal gas constant;
r, radial coordinate;
Sc_e, effective Schmidt number, defined by equation (7);
T, absolute temperature;
v_x, v_r, velocity components in direction of cylindrical coordinates x, r respectively;

* This work was supported by the State of California on Air Pollution Research Grant No. 40265. Computer time for the numerical calculations was provided by the Campus Computing Network of the University of California, Los Angeles.

† Presently at Jet Propulsion Laboratory, California Institute of Technology, Pasadena, California.

u, v, velocity components in direction of boundary layer coordinates x, y respectively;
u_τ, friction velocity $= \sqrt{\tau/\rho}$;
u^+, u/u_{τ_s};
W, rate of species production by chemical reaction;
x, mole fraction;
x, streamwise coordinate;
y, transverse coordinate measured from wall;
y^+, $u_{\tau_s} y/\nu$;
y^{++}, dimensionless value, defined by equation (18);
α, thermal diffusivity;
δ^*, displacement thickness;
$\varepsilon_M, \varepsilon_D, \varepsilon_H$, eddy diffusivity for transfer of momentum, mass species and heat, respectively;
ε^+, dimensionless momentum diffusivity, defined by equation (6);
ν, ν^+, kinematic viscosity, ν/ν_s;
ρ, ρ_{av}, mixture density, average value;
$\tau, \tau^{(r)}$, shear stress, reaction time of r'th reaction;
ψ, stream function;
ω, dimensionless radial coordinate, defined by equation (22).

Subscripts

b, bulk value;
e, free stream;
i, i'th species;
0, entrance value;
s, surface value;
t, ts, transferred states;
∞, fully developed.

INTRODUCTION

TURBULENT flows of chemically reacting gas mixtures inside ducts are encountered widely in engineering practice. The situations range from automobile afterburners to power plant stacks. In this paper, we present a numerical procedure for solving a broad range of turbulent tube flow problems which incorporates the effects of variable properties, surface mass transfer, and chemical reactions. Previous efforts to analyze such flows have utilized, in large measure, the so-called "film theory" of chemical engineering practice. For example, Brian and Reid [1] and Brian [2] used this approach, further simplifying the problem by linearizing the reaction rate expression. In support of their theories Brian *et al.* [3] investigated experimentally the effects of NO_2 decomposition on heat transfer from a turbulent boundary layer. The theory proved adequate only for a narrow range of the problem parameters. Presler [4] has reported an experimental study of heat transfer in turbulent tube flow for the N_2O_4–NO_2 system, the results showing, as expected, greatly enhanced heat transfer rates at the wall. By using frozen properties, it was found that the results could be correlated by an expression of the form recommended by Kays and Leung [5] for fully developed constant property flow, namely

$$Nu = \text{constant} \cdot Pr^{0.5} Re^{0.8}. \quad (1)$$

For turbulent flows with mass transfer at the wall, analyses of a few simple problems have appeared. For example, the uniform injection problem was solved by Yuan and Galowin [6], and that with exponential variation by Yuan and Brogren [7]. In both instances the effects, on turbulent transport, of such "disturbing factors" as variable properties and the surface mass transfer itself were ignored. More recently Kinney and Sparrow [8] analyzed locally self-similar turbulent tube flow with suction. Their eddy diffusivity model accounts for the effect of mass transfer on turbulent transport near the wall via a suitably modified van Driest damping factor. Experimental work on tube flows with injection has been reported by Yuan and Barazotti [9] and by Olson and Eckert [10].

Our numerical procedure involves direct solution, by finite difference methods, of the partial differential equations governing conservation of mass species, momentum and energy, and stems from the procedure proposed by Patankar and Spalding [11]. Since the axial

pressure gradient is *a priori* unknown, closure of the solution procedure centers about the treatment of the pressure gradient term in the momentum conservation equation. Recently, Bankston and McEligot [12] have analyzed entrance region heat transfer to variable property gases following exactly the closure prescription recommended in [11]. Libby *et al.* [13] calculated flow development in a tube with surface mass transfer but side-stepped the pressure gradient problem by invoking the highly restrictive assumption of isothermal flow. In the present solution procedure closure is obtained by performing overall mass and momentum balances on a control volume located between successive steps in the forward integration. An additional feature of our solution procedure is the incorporation of an improved eddy diffusivity model which accommodates near wall disturbances arising from property variations and surface mass transfer.

Solutions have been obtained for turbulent tube flows of non-reacting air, equilibrium mixtures of N_2O_4–NO_2, and nonequilibrium mixtures of NO_2–NO–O_2. The effects of surface mass transfer were studied for both the injection of inert air into air, and for the injection of O_2 into NO_2–NO–O_2 mixtures. Results are presented for the skin friction coefficient and pressure drop, the surface heat flux and the mass transfer conductance. Sample profiles of velocity, effective eddy diffusivity, temperature and mass fraction are also displayed. Where profitable, comparisons are made with experimental data.

ANALYSIS AND NUMERICAL PROCEDURE

Physical model and coordinate system

The physical situation and the coordinate system are depicted in Fig. 1. The hydrodynamic condition at the tube entrance is axisymmetric and time-mean steady, the velocity profile being either uniform or fully developed. The multicomponent gas mixture enters the tube in thermodynamic equilibrium, its temperature, pressure and chemical state being uniform across the flow. The entering flow is, for $x > 0$, perturbed by conditions at the wall, i.e. drag, surface mass transfer and changes in wall temperature. Illustrated in the figure are usual cylindrical coordinates (x, r) for axisymmetric flow; the corresponding velocity components are (v_x, v_r). Also shown are "boundary layer" coordinates (x, y), where $y = R - r$, with corresponding velocity components (u, v), where $u \equiv v_x$ and $v = -v_r$. The normalized cross-stream coordinate $0 < \omega < 1$ will be discussed later.

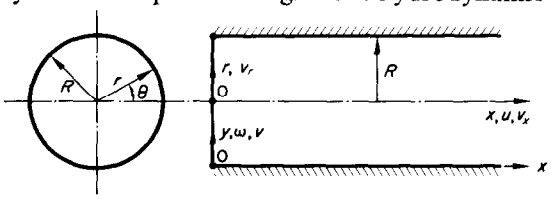

FIG. 1. Definition of coordinate systems.

Conservation equations

We assume that the multicomponent mixture is effectively binary with equal diffusion coefficients, and that second order correlations of the fluctuating components of the dependent variables can be approximated by introducing eddy diffusivities. The conservation equations are written in a form convenient to our purposes as

$$\frac{\partial}{\partial x}[\rho u(R-y)] - \frac{\partial}{\partial y}[\rho v_r(R-y)] = 0 \quad (2)$$

$$\rho u\frac{\partial u}{\partial x} - \rho v_r\frac{\partial u}{\partial y} = \frac{1}{(R-y)}\frac{\partial}{\partial y} \times \left[\rho\nu(R-y)\varepsilon^+\frac{\partial u}{\partial y}\right] - \frac{\mathrm{d}p}{\mathrm{d}x} \quad (3)$$

$$\rho u\frac{\partial m_i}{\partial x} - \rho v_r\frac{\partial m_i}{\partial y} = \frac{1}{(R-y)}\frac{\partial}{\partial y} \times \left[\frac{\rho\nu(R-y)}{Sc_e}\frac{\partial m_i}{\partial y}\right] + \dot{W}_i \quad (4)$$

$$\rho u\frac{\partial h}{\partial x} - \rho v_r\frac{\partial h}{\partial y} = \frac{1}{(R-y)}\frac{\partial}{\partial y}\left\{\rho\nu(R-y) \times \left[\frac{1}{Pr_e}\frac{\partial h}{\partial y} + \left(\frac{1}{Sc_e} - \frac{1}{Pr_e}\right)\sum_i h_i\frac{\partial m_i}{\partial y}\right]\right\} + u\frac{\mathrm{d}p}{\mathrm{d}x} + \rho\nu\varepsilon^+\left(\frac{\partial u}{\partial y}\right)^2 \quad (5)$$

where we have neglected

(i) axial diffusion of momentum, mass species and thermal energy,
(ii) body forces and cross-stream pressure gradients,
(iii) turbulent fluctuations in the transport properties, and
(iv) pressure and thermal diffusion and diffusional conduction.

The quantities ρ, u, v_r, p, h, etc., are time-averaged and the total dimensionless transport properties are defined as

$$\varepsilon^+ = 1 + \frac{\varepsilon_M}{\nu} \tag{6}$$

$$\frac{1}{Sc_e} = \frac{1}{\nu/\mathscr{D}} + \frac{1}{\nu/\varepsilon_D} \tag{7}$$

$$\frac{1}{Pr_e} = \frac{1}{\nu/\alpha} + \frac{1}{\nu/\varepsilon_H}. \tag{8}$$

In terms of the frozen specific heat $C_p = \sum_i m_i C_{pi}$, equation (5) may be written alternatively as

$$\rho u \frac{\partial T}{\partial x} - \rho v_r \frac{\partial T}{\partial y} = \frac{1}{(R-y)} \frac{\partial}{\partial y}\left[\frac{\rho\nu(R-y)}{Pr_e}\frac{\partial T}{\partial y}\right] + \frac{u}{C_p}\frac{\mathrm{d}p}{\mathrm{d}x} + \frac{\rho\nu\varepsilon^+}{C_p}\left(\frac{\partial u}{\mathrm{d}y}\right)^2 + \frac{\rho\nu}{C_p Pr_e}\frac{\partial T}{\partial y}\frac{\partial C_p}{\partial y} - \frac{1}{C_p}\sum_i h_i \dot{W}_i. \tag{9}$$

Boundary conditions for the flow are

at $y = R$:

$$v_r = \partial u/\partial y = \partial m_i/\partial y = \partial h/\partial y = \partial T/\partial y = 0 \tag{10}$$

at $y = 0$:

$$u = 0, \quad -\rho v_r \equiv \dot{m}(x)$$
$$\dot{m}m_{i,ts} = \dot{m}m_{i,s} + j_{i,s}$$
$$\dot{m}h_t = \dot{m}h_s + q_s \quad \text{or } T = T_s \tag{11}$$

where, for the moment, we write down after Spalding (e.g. see [14]), general expressions for conservation of mass species and energy at the wall. More specific forms of these boundary conditions will be stated later upon introducing the problem situations considered in this paper.

At $x = 0$ we considered two possibilities for the velocity profiles:

$$u(0, y) = u_0 = \nu Re_0/2R \tag{12}$$

or

$$u^+(0, y^+) = y^+ \text{ in the wall region}$$
$$u^+(0, y^+) = 8{\cdot}7(y^+)^{\frac{1}{7}} \text{ in the outer region} \tag{13}$$

where

$$u^+ = u/u_{\tau_s} = u/\sqrt{(\tau_s/\rho)}$$
$$y^+ = y\sqrt{(\tau_s/\rho)}/\nu$$
$$\tau_s/\rho = 0{\cdot}0395\, u_b^2 Re_0^{-\frac{1}{4}} = 0{\cdot}0395(\nu/2R)^2 Re_0^{\frac{7}{4}}.$$

For mass species

$$m_i(0, y) = m_{i,0} \text{ (equilibrium)} \tag{14}$$

and for thermal energy

$$T(0, y) = T_0. \tag{15}$$

Before discussing the overall method of solution, we present the eddy diffusivity formulation and specify the chemical systems considered.

Eddy diffusivity formulation

In the present treatment, ε_M, ε_D and ε_H are assumed equal and a new formulation for the dimensionless total diffusivity $\varepsilon^+ = 1 + \varepsilon_M/\nu$ is proposed. (The formulation is based on mixing length theory and extends the near wall result of van Driest [15]; thus, it applies as well to external flows.) From the definition of the friction velocity u_τ

$$u_\tau^2 \equiv (\sqrt{\tau/\rho})^2 = \nu(1 + \varepsilon_M/\nu)(\partial u/\partial y) = \nu\varepsilon^+ \partial u/\partial y$$

which result, when normalized with respect to wall values, becomes

$$(u_\tau^+)^2 = (u_\tau/u_{\tau_s})^2 = (\nu/\nu_s)(\varepsilon^+)\partial(u/u_{\tau_s})/\partial(yu_{\tau_s}/\nu_s)$$
$$= \nu^+\varepsilon^+\partial u^+/\partial y^+$$

where, paralleling van Driest,

$$\varepsilon^+ - 1 = \varepsilon_M/\nu = (K^{+2}y^{+2}/\nu^+)(\partial u^+/\partial y^+)$$

with, however, the added feature that the damping factor K^+ is defined such that y is made dimensionless using the local shear stress rather than the wall value:

$$K^+/K = 1\text{-}\exp[-y/(26\nu/u_\tau)] = 1\text{-}\exp[-y^+/(26\nu^+/u_\tau^+)]. \quad (16)$$

Eliminating $\partial u^+/\partial y^+$ from the above expressions,

$$\varepsilon^+ = \tfrac{1}{2}\{1 + [1 + 4(K^+y^{++})^2]^{\frac{1}{2}}\} \quad (17)$$

where

$$y^{++} = u_\tau^+ y^+/\nu^+. \quad (18)$$

We observe that equation (17) satisfies the basic requirement that $\varepsilon^+ = 1$ at the wall; furthermore, $\varepsilon^+ = K^+y^{++}$ as y^{++} becomes large. In addition, the Reichardt–Elrod criterion [16, 17] is also satisfied, namely, ε_M varies like y^4 as $y \to 0$.

Owing to the lack of a suitable rationale and a paucity of experimental data, an improved formulation for the outer flow was not pursued. Instead, Reichardt's expression [16] for tube flow,

$$\varepsilon^+ = 1 + G(y_i^+)[1 - (1 - y^+/R^+)^2][1 + 2(1 - y^+/R^+)^2] \quad (19)$$

was matched, through $G(y_i^+)$, to the inner expression. It is the matching procedure which is

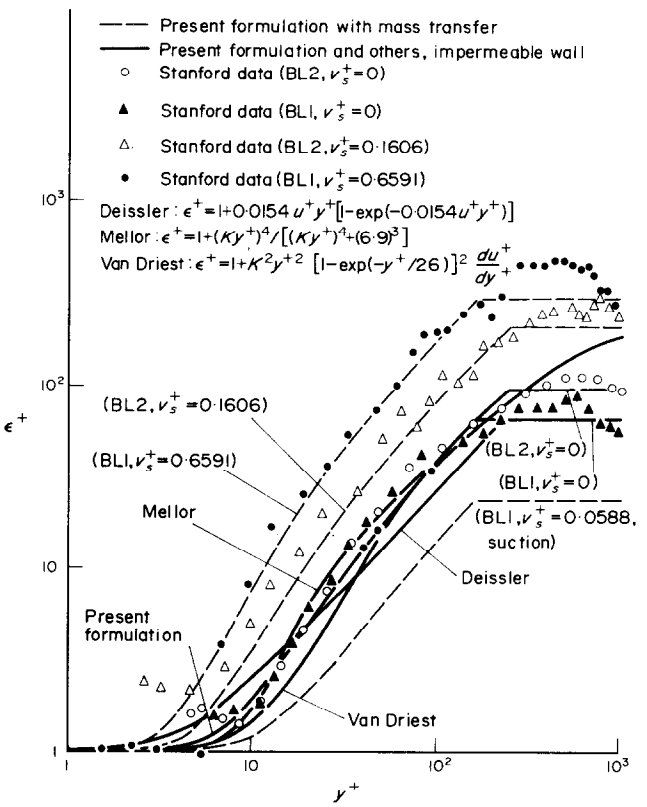

FIG. 2. Comparison of various effective diffusivity expressions for incompressible impermeable wall flows and for boundary layer flows with various mass transfer rates computed from the present formulation.

unique to the present formulation. By definition $R^+ = Ru_{\tau_s}/\nu$, and the function $G(y_i^+)$ depends on the particular flow situation, being equal to $KR^+/6$ for the special case of a constant property flow. In general, $G(y_i^+)$ would be determined by the requirement that ε^+ be continuous at the match point y_i^+. The actual value of y_i^+ hinges on the postulate that the choice yield a self-consistent interpretation of experimental data. We therefore assume that y_i^+ is independent of compressibility effects, physical property variations, pressure gradient, and surface mass transfer; the corresponding "undisturbed" flow is termed a "reference flow". The procedure for calculating the eddy diffusivity profile for a general flow is then

(i) Assign y_i^+ consistent with the requirement that ε^+ for the reference flow be continuous.

(ii) Obtain, in terms of y_i^+, $y_i^{+\,+}$ and hence ε_i^+ for the actual flow, using equations (17) and (18).

(iii) Introduce y_i^+ and ε_i^+ into equation (19) and solve for $G(y_i^+)$.

The above formulation has been used for examples of boundary layer as well as tube flows, with and without mass transfer at the wall. (For an external boundary layer equation (19), after Clauser [18], is replaced by the simpler form $\varepsilon^+ = 1 + F(y_i^+)$ where $F(y_i^+) = 0{\cdot}018\ u_e^+(\delta^*)^+$ for constant property flow along a flat plate.) Results are presented in Figs. 2–4 and comparisons are made, where possible, with the Stanford experimental data [19]. From Fig. 2, it is seen that for constant property boundary layer flows the present formulation is possibly an improvement over previous formulations. For injection the predictions remain satisfactory

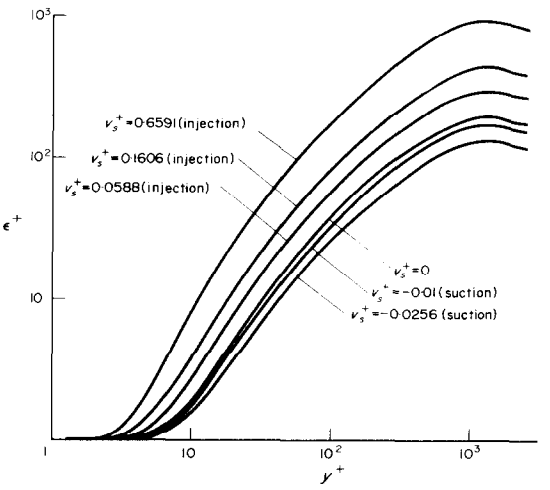

FIG. 3. Effective diffusivity computed from the new formulation for tube flows with various mass transfer rates.

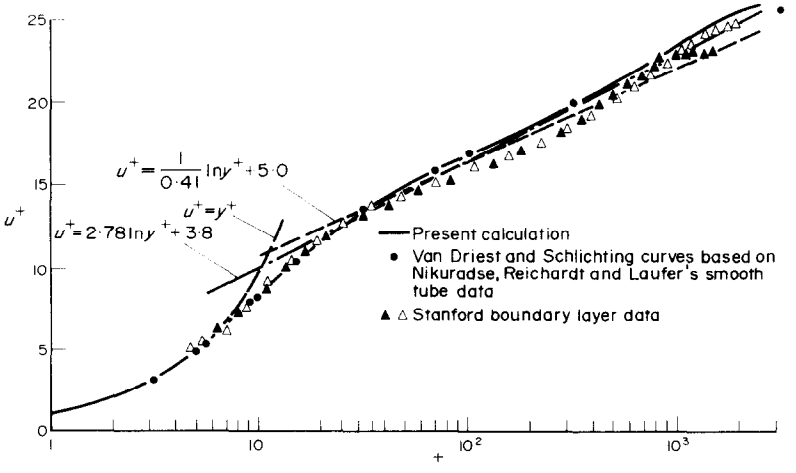

FIG. 4. Comparison of the resulting velocity profiles.

even at higher blowing rates. Although data are not available for comparisons with the tube flow predictions, Fig. 3 is included to illustrate the effects of injection. Figure 4 presents comparisons of velocity profiles as calculated by means of the present method with those obtained from the Stanford data and other formulations.

Chemical systems and wall conditions

In the present work, three distinct chemical systems were studied:

A. Non-reacting air

B. The equilibrium reaction (I):

$$N_2O_4 \rightleftharpoons 2NO_2$$

C. The nonequilibrium reaction (II):

$$2NO_2 \rightleftharpoons 2NO + O_2$$

For case C, the additional effect of heterogeneous reaction at the wall was included; while, for cases A and C the effects of injecting air and O_2, respectively, were studied.

With regard to reaction I, it is well known that the forward and reverse rate constants are very large, even at room temperature; furthermore, the reaction is essentially driven to completion as the temperature is increased before reaction II proceeds at measurable rates. Thus the reactions may be studied separately. With these points in mind, we now complete the mathematical formulation of the problems to be solved.

A. *Nonreacting air.* For this case, since air was the only species injected, equation (4) was not required and the wall boundary conditions were assigned as

$$\rho v\big|_{y=0} = \dot{m}(x)$$

and

$$T(x, 0) = T_s \text{ or } q(x, 0) = q_s.$$

B. *The equilibrium system* N_2O_4–NO_2. According to Giauque and Kemp [20], Bodenstein and Böes [21], and composition data as tabulated in Svhela and Brokaw [22], the equilibrium constant for reaction I is

$$K_p^{(I)} \equiv \frac{p x_{NO_2}^2}{x_{N_2O_4}} = \frac{p M M_{N_2O_4}}{M_{NO_2}^2} \cdot \frac{m_{NO_2}}{m_{N_2O_4}}$$
$$= 1{\cdot}6 \times 10^{12} \exp[-12\,000/T(^\circ\mathrm{R})]\ \mathrm{lb_f/ft^2}. \quad (20)$$

Since the homogeneous rate constants are large, catalytic effects at the wall are inconsequential; thus, equilibrium may be presumed throughout and equation (4) eliminated in favor of equation (20). Furthermore, for this case we chose not to consider mass transfer at the wall [$\dot{m}(x) = 0$] and assigned uniform wall temperatures [$T(x, 0) = T_s$], solving equation (9) rather than (5).

C. *The nonequilibrium system* NO_2–NO–O_2. According to Rosser and Wise [23] and Ashmore and Burnett [24], the decomposition of NO_2 is second order with rate expression

$$\frac{dc_{NO_2}}{dt} = -4 \times 10^{12}\, c_{NO_2}^2 \exp[-26\,900/\mathscr{R}T(^\circ\mathrm{K})]\ \mathrm{g\text{-}moles/cm^3 s}$$

from which the forward reaction rate constant was calculated to be

$$k_f^{(II)} = 3{\cdot}204 \times 10^{10} \exp[-24\,400/T(^\circ\mathrm{R})]\ \mathrm{ft^3/lb_m\text{-}mole\text{-}s}.$$

From [20–22]

$$K_p^{(II)} \equiv \frac{p x_{NO}^2 x_{O_2}}{x_{NO_2}^2} = \frac{p M M_{NO_2}^2}{M_{NO}^2 M_{O_2}} \cdot \frac{m_{NO}^2 m_{O_2}}{m_{NO_2}^2}$$
$$= 1{\cdot}6 \times 10^{11} \exp[-25\,000/T(^\circ\mathrm{R})]\ \mathrm{lb_f/ft^2}. \quad (21)$$

The above expressions hold for the temperature range $540^\circ\mathrm{R} < T < 2300^\circ\mathrm{R}$.

The resulting species production terms $\dot{W}_i$ are

$$\dot{W}_{NO_2} = -2\rho M_{NO_2}(K^{(II)} m_{NO_2}^2 - m_{NO}^2 m_{O_2})/\tau^{(II)}$$
$$\dot{W}_{NO} = -M_{NO}\dot{W}_{NO_2}/2M_{NO_2}$$
$$\dot{W}_{O_2} = -M_{O_2}\dot{W}_{NO_2}/2M_{NO_2}$$

where

$$K^{(II)} = M_{NO}^2 M_{O_2} K_p^{(II)}/p M M_{NO_2}^2$$

and

$$\tau^{(II)} = M_{NO}^2 M_{O_2} K_p^{(II)} / \rho p M k_f^{(II)}.$$

In addition to reaction II, catalytic effects at the wall, for a cupric-oxide on alumina catalyst, were investigated for which Wilkstrom and Nobe [25] and Sourirajan and Accomazzo [26] have shown that the rate constant for NO_2 decomposition is

$$k_w^{(II)} = 10^6 \exp[-30{,}400/T(^\circ R)]\, lb_m/ft^2 s.$$

In such an event, we will term the wall "partially catalytic"; otherwise the wall will be termed "non-catalytic" or "fully catalytic" (reaction II in equilibrium).

Based on the above discussion, the boundary conditions for equation (4) are (noting that one species equation is redundant)

$$m_{NO_2,ts} = m_{NO,ts} = 0; m_{O_2,ts} = 1$$

for the non-catalytic wall. For the fully catalytic wall

$$m_{NO}^2 m_{O_2} / m_{NO_2}^2 = K^{(II)}$$

$$m_{NO,ts} = -M_{NO} m_{NO_2,ts} / M_{NO_2}$$

$$m_{NO_2} + m_{NO} + m_{O_2} = 1$$

while for the partially catalytic wall,

$$m_{NO_2,ts} \dot{m} = k_w^{(II)}$$

$$m_{NO,ts} \dot{m} = -M_{NO} k_w^{(II)} / M_{NO_2}$$

$$m_{NO_2} + m_{NO} + m_{O_2} = 1.$$

The thermal boundary condition, applied to equation (9), was $T = T_s$ which in all cases was taken to be constant.

Thermophysical properties

The thermodynamic properties were computed assuming an ideal gas mixture. The individual specific heats were obtained from the JANAF tables [27], while their heats of formation were taken from Svhela and Brokaw [22]. Transport properties for the individual species were computed according to the Chapman–Enskog kinetic theory of gases. The Lennard–Jones interaction potential was assumed with the force constants taken from [28]. The mixture viscosity was computed according to Wilke [29], the frozen thermal conductivity according to Mason and Saxena [30] (dropping the factor 1·065), and the effective diffusion coefficient by means of an arithmetic average of the binary values.

Method of solution

A detailed treatment is given in [31]; briefly the method of solution was as follows. Equations (2)–(4) and (5) or (9) were reformulated in terms of coordinates (x, ω) where

$$\omega^2 = (\psi - \psi_s)/(\psi_R - \psi_s) = \int_0^y \rho u (R - y) \mathrm{d}y / \Delta\psi \tag{22}$$

and the stream function ψ satisfies the relations

$$\rho u (R - y) = \partial\psi/\partial y \text{ and } \rho v (R - y) = \partial\psi/\partial x.$$

Use of equation (22), as shown in [32], enables more accurate numerical solutions than the familiar Patankar–Spalding transformation [11] since $\partial u/\partial\omega = [2\omega\Delta\psi/\rho u(R - y)]\partial u/\partial\omega$ and, for that matter, all ω-derivatives remain bounded as $\omega \to 0$. Such is not the case for the P–S transformation, where relatively larger truncation errors in finite difference approximations of the transformed equations are introduced at node-points near the wall. The nonlinear transformation has the added advantage that the accuracy of wall gradients, which are extracted from polynomial fits to the near-wall numerical data directly in the x-ω plane, for example,

$$\partial u/\partial y\,|_{y=0} = \lim_{\omega \to 0} [\rho u (R - y)/2\omega\Delta\psi]\partial u/\partial\omega$$

$$= (\rho u R/2\Delta\psi)(\partial u/\partial\omega)^2$$

is consistent with that of the numerical data itself.

From equation (22) it is seen that $(R - y)\mathrm{d}y = 2\omega\Delta\psi \mathrm{d}\omega/\rho u$ and hence, that

$$y = R - \sqrt{[R^2 - 4\Delta\psi \int_0^\omega (\omega/\rho u)\mathrm{d}\omega]}. \tag{23}$$

In these terms, it may easily be shown that equations (3)–(5) and (9) assume the general form

$$\frac{\partial V_n}{\partial x} - \frac{1}{\omega}\frac{\partial}{\partial \omega}\left[F(\psi)V_n\right] - \frac{V_n}{\Delta\psi}\frac{\mathrm{d}\psi_s}{\mathrm{d}x} = \frac{1}{\omega}\frac{\partial}{\partial \omega}\left(\frac{C_n\phi}{\omega}\frac{\partial V_n}{\partial \omega}\right) + S_n \quad (24)$$

where

$$F(\psi) = \frac{1}{2\Delta\psi}\left(\frac{\mathrm{d}\psi_s}{\mathrm{d}x} + \omega^2\frac{\mathrm{d}\Delta\psi}{\mathrm{d}x}\right) \quad (25)$$

and

$$\phi = (\rho v)(\rho u)\left[(R - y)/2\Delta\psi\right]^2. \quad (26)$$

The quantities V_n, C_n and S_n are defined in Table 1.

where $i = 2, 3 \ldots, I-1$; $i = 1$ denoting the tube wall and $i = I$ the centerline. For $i = 2$ or $I - 1$, boundary values for V_n are introduced on the right hand side of equation (27). When these are unknown in advance, as is the case in general at $\omega = 1$ and, depending on the wall boundary condition specified, occasionally at $\omega = 0$, they are eliminated algebraically in terms of forward difference expressions involving values at the interior node points, for example,

$$V_{n,1,j} = \alpha_{j-1}\, V_{n,2,j} + \beta_{j-1}\, V_{n,3,j} + \gamma_{j-1}. \quad (28)$$

The numerical solution was advanced, without

Table 1. Identification of dependent variables V_n, *coefficients* C_n, *and source terms* S_n *in equation* (24)

n	V_n	C_n	S_n
1	u	ε^+	$-(\mathrm{d}p/\mathrm{d}x)/\rho u$
2–5	m_i	Sc_e^{-1}	$\dot{W}_i/\rho u$
6	T	Pr_e^{-1}	$\frac{1}{C_p}\left\{\frac{1}{\rho}\frac{\mathrm{d}p}{\mathrm{d}x} - \frac{1}{\rho u}\sum_i h_i\dot{W}_i + \phi\varepsilon^+\left(\frac{1}{\omega}\frac{\partial u}{\partial \omega}\right)^2 + \frac{\phi}{Pr_e}\frac{1}{\omega^2}\frac{\partial T}{\partial \omega}\frac{\partial C_p}{\partial \omega}\right\}$
7	h	Pr_e^{-1}	$\frac{1}{\omega}\frac{\partial}{\partial \omega}\left[\frac{\phi}{\omega}\left(\frac{1}{Sc_e} - \frac{1}{Pr_e}\right)\sum_i h_i\frac{\partial m_i}{\partial \omega}\right] + \frac{1}{\rho}\frac{\mathrm{d}p}{\mathrm{d}x} + \phi\varepsilon^+\left(\frac{1}{\omega}\frac{\partial u}{\partial \omega}\right)^2$

Equation (24) was solved numerically using finite difference methods. Briefly, this was done as follows. The cross-stream derivatives were approximated by means of implicit three-point difference analogs in terms of node point locations (x_j: ω_{i-1}, ω_i, ω_{i+1}), linearizing the resulting algebraic forms by evaluating position-dependent coefficients at the upstream station x_{j-1}. Upon introducing a backward difference expression for $\partial V_n/\partial x$, evaluating the source terms upstream, and collecting terms, equation (24) assumes the algebraic form

$$V_{n,i,j} = A_{n,i,j-1}\, V_{n,i+1,j} + B_{n,i,j-1}\, V_{n,i-1,j} + D_{n,i,j-1} \quad (27)$$

iteration, from x_{j-1} to x_j as follows:

(i) Obtain, by means of the expression $\Delta\psi_j = \Delta\psi_{j-1} - \int_{x_{j-1}}^{x_j} \dot{m}R\,\mathrm{d}x$, the mass flow rate at x_j.

(ii) Extract, by means of an overall momentum balance (see discussion below), the axial pressure gradient $\mathrm{d}p/\mathrm{d}x$.

(iii) Compute coefficients $A_{n,i,j-1}$, $B_{n,i,j-1}$ and $D_{n,i,j-1}$, modifying as required the coefficients at $i = 2$ or $I - 1$ as suggested by eliminating, say, $V_{n,1,j}$ in equation (27) by means of equation (28).

(iv) Solve, by means of successive substitution [11], the set of algebraic equations (27).
(v) Calculate $V_{n,I,j}$ and, depending on the type of boundary condition at the wall, $V_{n,1,j}$ or $j_{n,1,j}$.
(vi) Calculate, by means of equation (23), values of $y_{i,j}$ corresponding to the fixed set of node points ω_i.
(vii) Repeat steps (i)–(vi).

Axial pressure gradient

As mentioned above, dp/dx was extracted from an overall momentum balance. The expression used

$$-\frac{dp}{dx}=\frac{4}{y_{I,j-1}^2+R^2}\left\{\frac{2}{\bar{\rho}_j(x_j-x_{j-1})}\left[\left(\frac{\Delta\psi_j}{R}\right)^2-\left(\frac{\Delta\psi_{j-1}}{y_{I,j-1}}\right)^2\frac{\bar{\rho}_j}{\bar{\rho}_{j-1}}\right]+y_{I,j-1}\,\tau_{s,j-1}\right\} \quad (29)$$

where

$$\bar{\rho}=\int_0^R \rho u(R-y)\mathrm{d}y\Big/\int_0^R u(R-y)\mathrm{d}y$$

was structured so as to maintain $y_I \doteq R$. (To avoid iteration, $\bar{\rho}_j$ was obtained in terms of a weighted linear combination of $\bar{\rho}_{j-2}$ and $\bar{\rho}_{j-1}$.)

Note that if by numerical error $y_{I,j-1} < R$, $|dp/dx|$ will be reduced for the next computational step and the correct value, R, will be approached. For $y_{I,j-1} > R$ the opposite is true. Thus, using equation (29) not only gives a proper closure to the mathematical problem, but also provides means for stabilizing the numerical procedure.

RESULTS AND DISCUSSION

The numerical method developed allows engineering data to be obtained for a very wide range of problems. Our intention here is not to

Table 2. Case specifications for nonreacting air

Identification	Entrance Reynolds number	Thermal conditions		Remarks	
		Entrance (°R)	Wall (°R)		
A1	$5{\cdot}76\times10^3$	560	560	Hydrodynamically developing with zero mass injection	
A2	$1{\cdot}15\times10^4$	560	560		
A3	$4{\cdot}63\times10^4$	560	560		
A4	$9{\cdot}21\times10^4$	560	560		
A5	$2{\cdot}76\times10^5$	560	560		
A6	$8{\cdot}29\times10^5$	560	560		
A7	$1{\cdot}26\times10^6$	560	560		
				(v_s/u_b)	
				Initial	$(x/D) = 31{\cdot}3$
A8	$4{\cdot}63\times10^4$	560	560	0	0
A9	$4{\cdot}63\times10^4$	560	560	$1{\cdot}41\times10^{-3}$	$1{\cdot}20\times10^{-3}$
A10	$4{\cdot}63\times10^4$	560	560	2·82	2·08
A11	$4{\cdot}63\times10^4$	560	560	4·22	2·76
A12	$4{\cdot}63\times10^4$	560	560	5·63	3·36
A13	$4{\cdot}63\times10^4$	560	560	8·44	4·10
A14	$5{\cdot}76\times10^3$	560	600	$Pr = 0{\cdot}721$	
A15	$1{\cdot}15\times10^4$	560	600	$Pr = 0{\cdot}721$	
A16	$4{\cdot}63\times10^4$	560	600	$Pr = 0{\cdot}721$	
A17	$5{\cdot}55\times10^5$	560	600	$Pr = 0{\cdot}721$	
A18	$1{\cdot}26\times10^6$	560	600	$Pr = 0{\cdot}721$	
A19	$4{\cdot}63\times10^4$	560	$-0{\cdot}1$ Btu/ft²s	$Pr = 0{\cdot}721$	

present such data, but rather to demonstrate the versatility of the method with selected results for a variety of situations. In order to gain confidence in the numerical procedures, comparisons will be made with established prediction formulae and experimental data. Tables 2–4 present the detailed specifications of the flow cases considered. The serial letters A, B and C are used to designate the nonreacting, the equilibrium and the nonequilibrium systems, respectively. The numerical procedures are considered to be accurate to within a few per cent and unquestionably are as accurate as the physical property information and the chemical kinetics.

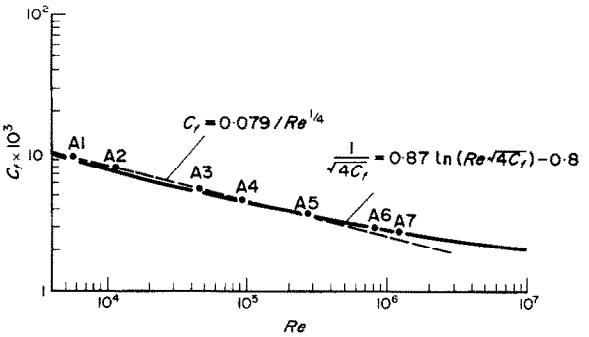

FIG. 5. Skin friction coefficient vs. Reynolds number (air).

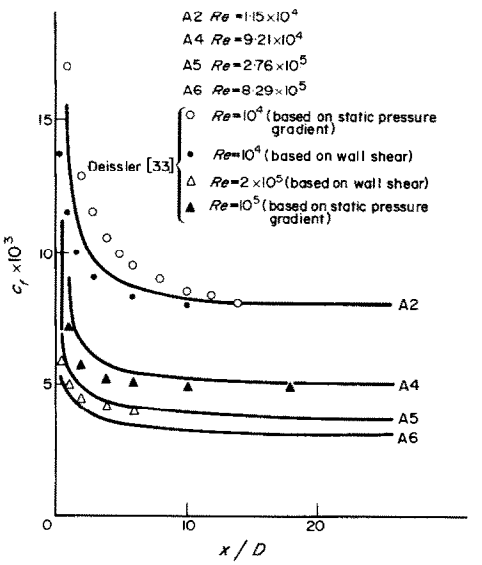

FIG. 6. Skin friction coefficient vs. x/D for various Reynolds numbers (air).

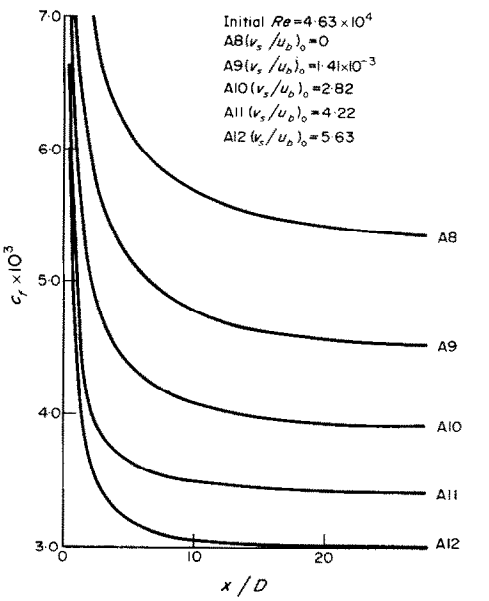

FIG. 7. Skin friction coefficient vs. x/D for various injection rates (air).

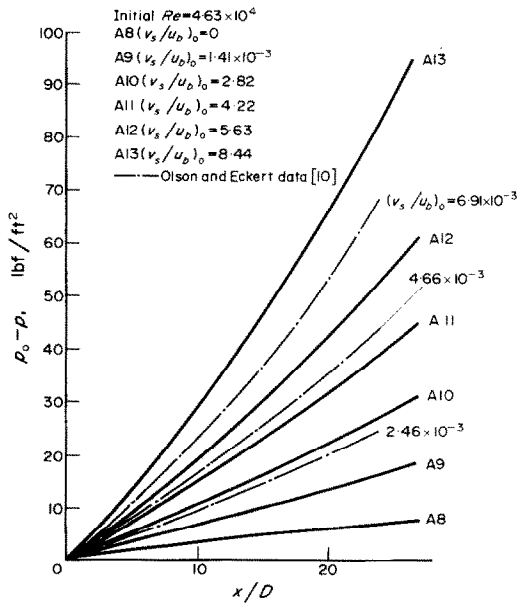

FIG. 8. Pressure drop vs. x/D for various injection rates (air).

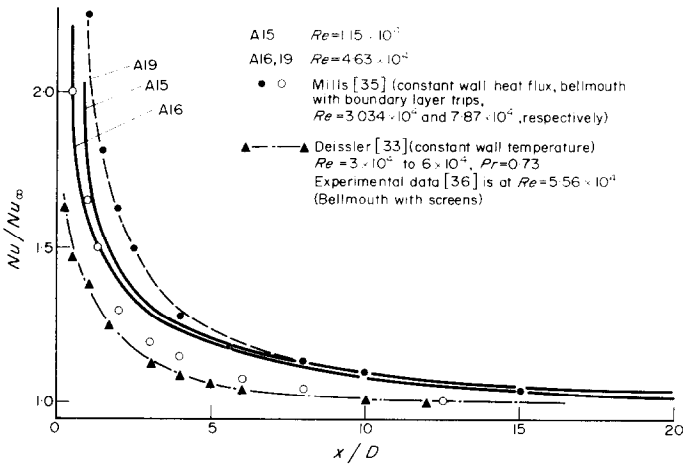

FIG. 9. Nusselt number ratio for simultaneous development of hydrodynamic and thermal entrance region (air).

The dimensionless groups, in terms of which momentum, mass and heat transfer data are conventionally presented, involve fluid properties. For variable property, chemically reacting, flows the appropriate condition at which these properties should be evaluated is not at all self-evident. For example, the temperature and composition could be evaluated as bulk values, wall values, or at some empirical reference state. Thus the Nusselt number tends to lose much of its significance for chemically reacting flows, though, casting results in this form does allow qualitative comparison of reacting flow data with the established correlations for inert flow. For reacting flows the viewpoint is taken here that it is actual wall shear stress, wall heat flux, etc., which are of the greatest importance and thus should be easily recoverable from the dimensionless correlations. Since, in most of the

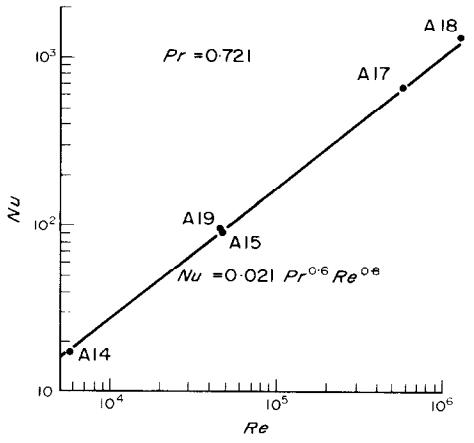

FIG. 10. Nusselt number vs. Reynolds number (air).

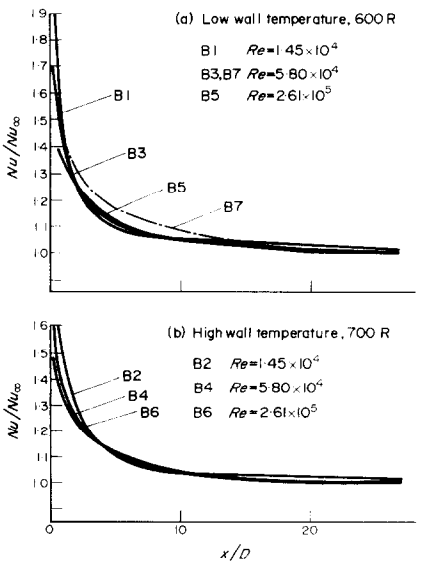

FIG. 11. Nusselt number ratio based on conduction wall heat flux vs. x/D ($N_2O_4 \leftrightharpoons 2NO_2$).

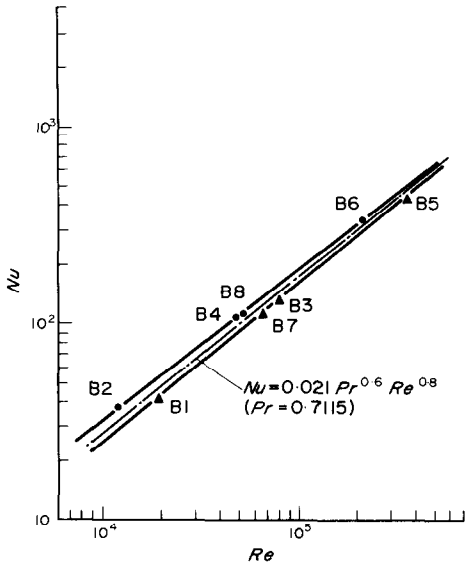

FIG. 12. Nusselt number based on conduction wall heat flux vs. Reynolds number ($N_2O_4 \leftrightharpoons 2NO_2$).

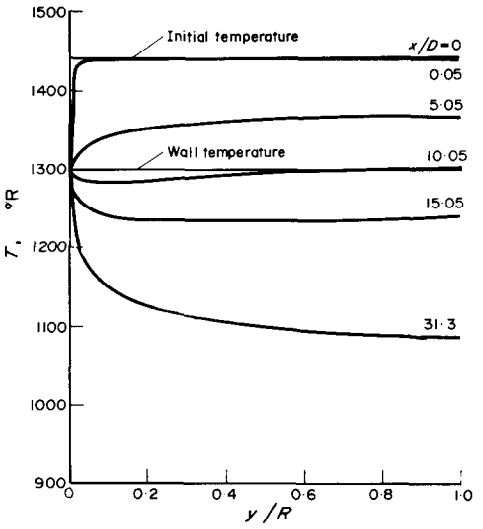

FIG. 14. Temperature profiles at various x/D for low wall temperature case C7 with injection of O_2 ($2NO_2 \leftrightharpoons 2NO + O_2$).

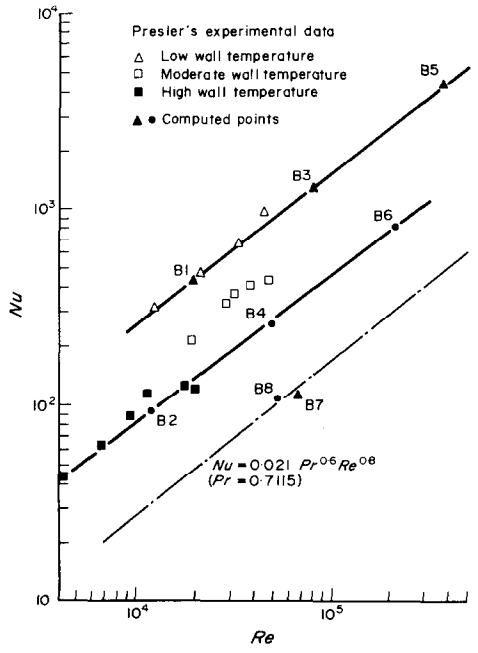

FIG. 13. Nusselt number based on total wall heat flux vs. Reynolds number ($N_2O_4 \leftrightharpoons 2NO_2$).

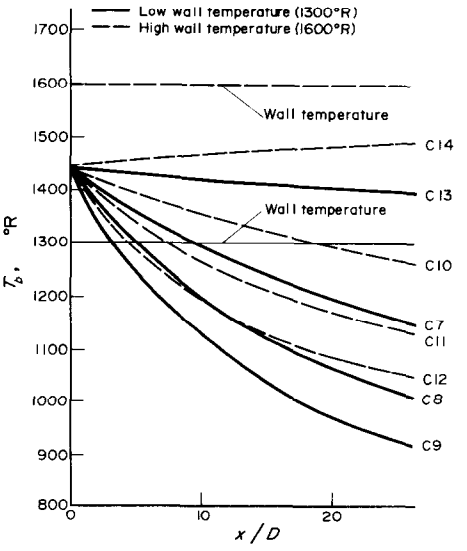

FIG. 15. Comparison of bulk temperature drop in streamwise direction for low and high wall temperature cases at various injection rates of O_2 ($2NO_2 \leftrightharpoons 2NO + O_2$).

cases studied, the wall temperature was specified, properties were evaluated at the wall temperature. An exception was the skin friction coefficient C_f which was defined in terms of the bulk density as it was expected that good agreement with nonreacting flow correlations could be thereby obtained. The computed data for the three chemical systems are presented in Figs. 5–19. A brief discussion of these results follows.

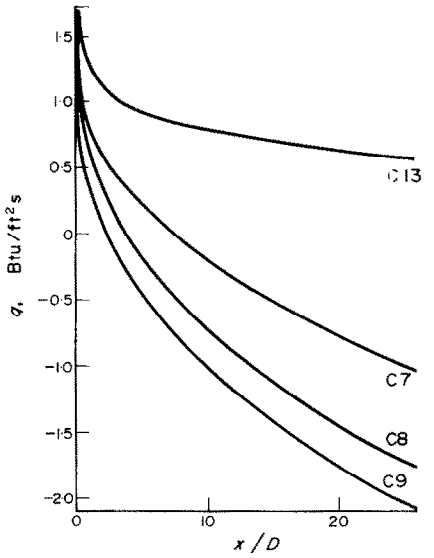

FIG. 16. Conduction wall heat flux vs. x/D for various injection rates of O_2—low wall temperature ($2NO_2 \leftrightharpoons 2NO + O_2$).

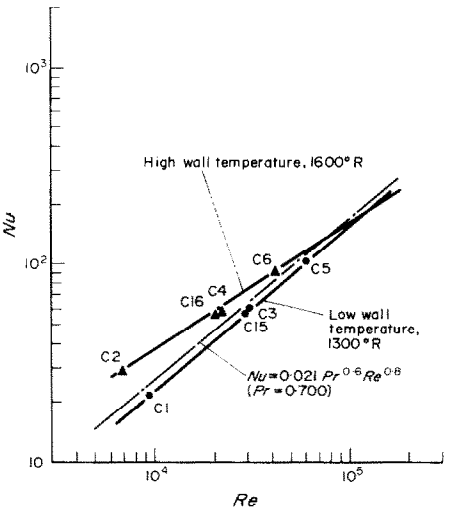

FIG. 18. Nusselt number based on conduction wall heat flux vs. Reynolds number ($2NO_2 \leftrightharpoons 2NO + O_2$).

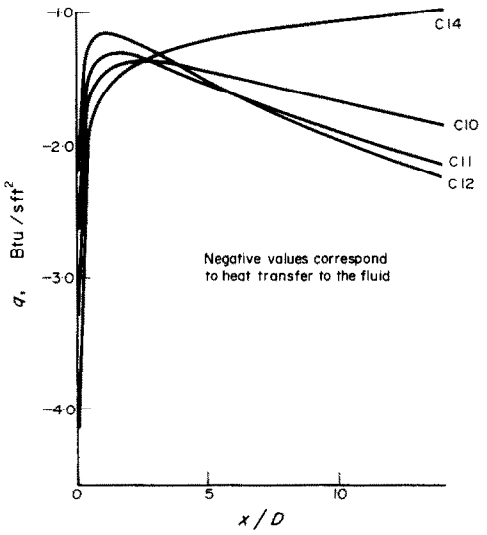

FIG. 17. Conduction wall heat flux vs. x/D for various injection rates of O_2—high wall temperature ($2NO_2 \leftrightharpoons 2NO + O_2$).

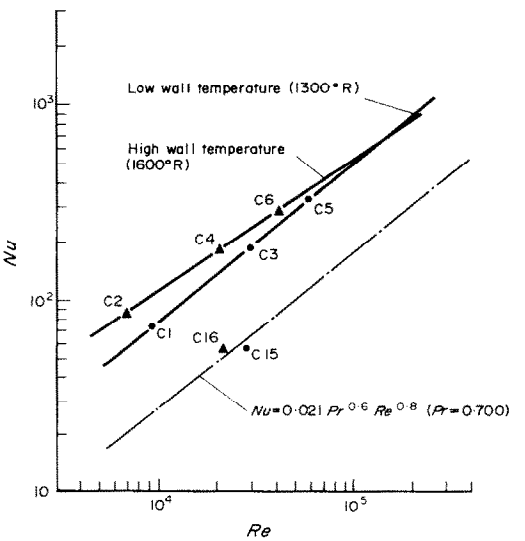

FIG. 19. Nusselt number based on total wall heat flux vs. Reynolds number ($2NO_2 \leftrightharpoons 2NO + O_2$).

A. *Nonreacting air (constant properties).* The results for air flow are shown in Figs. 5–10. Figure 5 compares the fully developed skin friction coefficients to the Blasius formula in its range of validity, and the accepted correlation for smooth tubes at higher Reynolds numbers; the agreement is excellent. Figure 6 shows the approach of C_f to the fully developed value, as x/D becomes large, for various Reynolds numbers. Some of the results of Deissler [33], as given by Knudsen and Katz [34], are also shown. Deissler computed two different skin friction coefficients, one based on the local wall shear and the other on the local static pressure gradient; these differ by the momentum change associated with the developing velocity profile in the entrance region. The present results lie between these two values, and indicate a slightly longer entry region. Considering the detailed differences in which the calculations were initialized, the comparison is satisfactory.

The results for injection into a hydrodynamically developing entrance region flow are shown in Figs. 7 and 8. In Fig. 8 a comparison is made with the experimental data of Olson and Eckert [10]; the agreement is satisfactory in view of the fact that, in the experiments, the flow was fully developed hydrodynamically before injection commenced. A more direct comparison with the data of [10] was not possible since, although a wide range of Reynolds number was covered, the values were not specifically indicated in this paper.

Figure 9 shows the results for simultaneous thermal and hydrodynamic development, in the form of the ratio Nu/Nu_∞ as a function of x/D, for both uniform wall temperature and uniform heat flux. Also shown are some analytical predictions of Deissler [33] and experimental data of Mills [35]. The discrepancies are partially due to a difference in Reynolds number, but more due to the nature of the boundary layer trip employed, as explained in [35]. The uniform wall temperature predictions of Deissler [33], which agree very well with the experimental data of Boelter *et al.* [36], lie well below the results of the present calculations. But it must be noted that Boelter *et al.*, used a bellmouth entrance with screens to trigger transition at the entrance; as noted in [35], this procedure is not as effective as boundary layer trips and thus the present results may better represent the flow situation under consideration.

The fully developed Nusselt number for a uniform wall temperature is shown in Fig. 10 for various Reynolds numbers. The results agree well with the Kays correlation [14], equation (1). One data point for uniform wall heat flux is also shown. The latter value is seen to be slightly higher than those for uniform wall temperature. This result is consistent with the

Table 3. Case specifications for the equilibrium system $N_2O_4 \rightleftharpoons 2NO_2$

Identification	Entrance Reynolds number	Thermal conditions		Chemical state
		Entrance (°R)	Wall (°R)	
B1	$1{\cdot}45 \times 10^4$	648	600	Equilibrium reaction, fully catalytic wall
B2	$1{\cdot}45 \times 10^4$	648	700	
B3	$5{\cdot}80 \times 10^4$	648	600	
B4	$5{\cdot}80 \times 10^4$	648	700	
B5	$2{\cdot}61 \times 10^4$	648	600	
B6	$2{\cdot}61 \times 10^4$	648	700	
B7	$5{\cdot}80 \times 10^4$	648	600	Frozen flow, noncatalytic wall
B8	$5{\cdot}80 \times 10^4$	648	700	

Kays correlations (a coefficient of 0·021 for uniform temperature and 0·022 for uniform heat flux). All the fully developed values are at $x/D = 31{\cdot}3$.

B. *The equilibrium system* $N_2O_4 \rightleftharpoons 2NO_2$. The results for this system are shown in Figs. 11–13. Figure 11 shows the variation, in the entrance region, of the Nusselt number based on the conduction component of the surface energy flux, $Nu = [\partial(T - T_s/T_s - T_b)/\partial(y/D)]_s$. As before, Nu_∞ is taken as the value of Nu at $x/D = 31{\cdot}3$. The behavior of Nu is similar for both cooling, Fig. 11(a), and heating, Fig. 11(b). In both cases, at lower Reynolds numbers, the Nusselt number approaches the fully developed value more rapidly at small x/D. It may also be noted by comparing Figs. 9 and 11, that the thermal development is more rapid in the case of chemical reaction as compared with non-reacting flow.

The fully developed Nusselt numbers based on conduction heat flux and total heat flux are shown in Figs. 12 and 13 respectively. The former is seen to be well correlated by the formula suggested by Kays [14], i.e. equation (1) with the proportionality constant equal to 0·021. However, the curve for cooling does lie slightly below the curve for heating; the curves tend to merge at high Reynolds numbers. This effect is due to property changes induced by variations in composition and temperature. If attention is directed to the runs with the same initial Reynolds number, it can be seen that the resulting Nusselt number is actually higher in the case of cooling (due to a decrease in thermal conductivity). However, the increase in Reynolds number (due to a decrease in viscosity) overshadowed the thermal conductivity effect. Figure 13 indicates that the Nusselt number based on the total heat flux is much higher than that based on the conduction heat flux only. The additional contribution is of course due to species interdiffusion in the equilibrium mixture. It is clear from the figure that a Kays type correlation can still be used provided the proportionality constant is modified. It can also be seen that the Nusselt number in the case of cooling has the highest value and agrees very well with Presler's [4] experimental data for low wall temperatures. The Nusselt number for heating is much lower and agrees well with Presler's data for high wall temperatures. It is noted that Presler's experiments were conducted under uniform wall heat flux conditions with the wall temperature varying from 650° to 1030°R.

C. *The nonequilibrium system* $2NO_2 \rightleftharpoons 2NO + O_2$. The results for this chemical system are shown in Figs. 14–19. The detailed specifications of the individual cases are listed in Table 4, where it may be seen that there are two major groups: one with injection of O_2, and the other with zero mass transfer. Figure 14 illustrates the typical development of the temperature profiles, at various x/D locations, for the low wall temperature case and injection of O_2. It is seen that the temperature profiles first lie above, but then gradually fall below the wall temperature level. This leads to the wall heat flux situation shown in Fig. 16, which indicates that heat is initially transferred from the fluid, but finally reverses direction and is transferred to the fluid. This behavior is initially due to both the cooling effect of the injectant and the acceleration in the streamwise direction; later of course only the latter effect is present. This behavior can also be seen from Fig. 15, which shows the bulk temperature change in the flow direction, and from Fig. 17 which is the conduction wall heat flux at various x/D positions for the high wall temperature case. Particularly noteworthy are the marked effects of injection on the bulk temperature, and the heat flux change in the vicinity of $x/D = 1$–3.

The fully developed Nusselt numbers based on conduction heat flux and on total wall heat flux are shown in Figs. 18 and 19 respectively. Figure 18 shows that the low wall temperature data are well correlated by the Kays formula, whereas the correlation of the high wall temperature data is not as good. Again the Nusselt number based on total wall heat flux exhibits the

Table 4. Case specifications for the nonequilibrium system $2NO_2 \rightleftharpoons 2NO + O_2$

Identification	Entrance Reynolds number	Thermal condition		Chemical State	Remarks	
		Entrance (°R)	Wall (°R)			
C1	$8{\cdot}22 \times 10^3$	1440	1300	Nonequilibrium reaction with a fully catalytic wall	No mass transfer	
C2	$8{\cdot}22 \times 10^3$	1440	1600		No mass transfer	
C3	$2{\cdot}47 \times 10^4$	1440	1300		No mass transfer	
C4	$2{\cdot}47 \times 10^4$	1440	1600		No mass transfer	
C5	$4{\cdot}93 \times 10^4$	1440	1300		No mass transfer	
C6	$4{\cdot}93 \times 10^4$	1440	1600		No mass transfer	
					$\dot{m}/\rho_b u_b$	
					Initial	$x/D = 31{\cdot}3$
C7	$2{\cdot}47 \times 10^4$	1440	1300	Nonequilibrium reaction with a fully catalytic wall	$2{\cdot}55 \times 10^{-3}$	$1{\cdot}93 \times 10^{-3}$
C8	$2{\cdot}47 \times 10^4$	1440	1300		$5{\cdot}10$	$3{\cdot}11$
C9	$2{\cdot}47 \times 10^4$	1440	1300		$7{\cdot}64$	$3{\cdot}91$
C10	$2{\cdot}47 \times 10^4$	1440	1600		$2{\cdot}55$	$1{\cdot}93$
C11	$2{\cdot}47 \times 10^4$	1440	1600		$5{\cdot}10$	$3{\cdot}11$
C12	$2{\cdot}47 \times 10^4$	1440	1600		$7{\cdot}64$	$3{\cdot}91$
C13	$2{\cdot}47 \times 10^4$	1440	1300		No mass transfer	
C14	$2{\cdot}47 \times 10^4$	1440	1600		No mass transfer	
C15	$2{\cdot}47 \times 10^4$	1440	1300	Frozen flow with a noncatalytic wall	No mass transfer	
C16	$2{\cdot}47 \times 10^4$	1440	1600		No mass transfer	

same trend as that based on the conduction flux, but is at a much higher level.

CONCLUSIONS

Our results show that the present numerical method and resulting computer program is quite satisfactory for the types of problems under consideration. For all the chemical systems, which included nonreacting air, the equilibrium system $N_2O_4 \rightleftharpoons 2NO_2$ and the nonequilibrium system $2NO_2 \rightleftharpoons 2NO + O_2$, the agreement with experimental data is satisfactory. The accuracy is more than adequate for engineering purposes. We conclude that the program will indeed serve the purpose of providing a general and economical method for solving turbulent tube flow problems with chemical reactions and surface mass transfer. It is expected that the program can be easily used for other chemical systems of a similar nature to those considered here.

From the inherent assumptions and special techniques incorporated into the final program, the following conclusions may be drawn

(i) For turbulent tube flow problems, in which the flow variables do not change too rapidly in the streamwise direction, linearization of the governing partial differential equations by evaluating the coefficients and source terms at the upstream station, and solution of the difference equations by a forward marching technique, yields results which are accurate enough for engineering purposes.

(ii) The evaluation of the pressure gradient term in the momentum conservation equation by means of mass and momentum balances between consecutive stations is a correct closure of the problem. The use of a slightly variable cross-sectional area in the momentum balance is an effective method for stabilizing the numerical computation.

(iii) The present formulation for the eddy diffusivity and the procedures for its

computation for the complete flow region of a boundary layer like flow appear to be quite satisfactory.

REFERENCES

1. P. L. T. BRIAN and R. C. REID, Heat transfer with simultaneous chemical reaction: film theory for a finite reaction rate, *A.I.Ch.E. Jl* **8**, 322–329 (1962).
2. P. L. T. BRIAN, Turbulent pipe flow heat transfer with a simultaneous chemical reaction of finite rate. *A.I.Ch.E. Jl* **9**, 831–841 (1963).
3. P. L. T. BRIAN, R. C. REID and S. W. BODMAN, Heat transfer to decomposing nitrogen dioxide in a turbulent boundary layer, *A.I.Ch.E. Jl* **11**, 809–814 (1965).
4. A. F. PRESLER, An experimental investigation of heat transfer to turbulent flow in smooth tubes for the reacting N_2O_4–NO_2 system, NASA TN D-3230 (1966).
5. W. M. KAYS and E. Y. LEUNG, Heat transfer in annular passages-hydrodynamically developed turbulent flow with arbitrarily prescribed heat flux, *Int. J. Heat Mass Transfer* **6**, 537–557 (1963).
6. S. W. YUAN and L. S. GALOWIN, Transpiration cooling in the turbulent flow through a porous-wall pipe, *Ninth Int. Congr. Appl. Mech.* **2**, 331–344 (1957).
7. S. W. YUAN and E. W. BROGREN, Turbulent flow in a circular pipe with porous wall, *Physics Fluids* **4**, 368–372 (1961).
8. R. B. KINNEY and E. M. SPARROW, Turbulent flow, heat transfer, and mass transfer in a tube with surface suction, *J. Heat Transfer* **92**, 117–125 (1970).
9. S. W. YUAN and A. BARAZOTTI, Experimental investigation of transpiration cooling in turbulent pipe flow, Polytechnic Institute of Brooklyn, PIBAL Report No. 479 (1958).
10. R. M. OLSON and E. R. G. ECKERT, Experimental studies of turbulent flow in a porous circular tube with uniform fluid injection through the tube wall, *J. Appl. Mech.* **88**, 7–17 (1966).
11. S. V. PATANKAR and D. B. SPALDING, *Heat and Mass Transfer in Boundary Layers*. Morgan-Grampian, London (1967).
12. C. A. BANKSTON and D. M. MCELIGOT, Turbulent and laminar heat transfer to gases with varying properties in the entry region of circular ducts, *Int. J. Heat Mass Transfer* **13**, 319–344 (1970).
13. P. A. LIBBY, T. M. LIU and F. A. WILLIAMS, Flow development in a tube with injection of a light or heavy gas, *Int. J. Heat Mass Transfer* **12**, 1267–1279 (1969).
14. W. M. KAYS, *Convective Heat and Mass Transfer*. McGraw-Hill, New York (1966).
15. E. R. VAN DRIEST, On turbulent flow near a wall, *J. Aeronaut. Sci.* **23**, 1007–1011 (1955).
16. H. Reichardt, Vollständige Darstellung der turbulenten Geschwindigkeitsverteilung in glatten Leitungen, *ZAMM* **31**, 208–219 (1951).
17. H. G. ELROD, JR., Note on the turbulent shear stress near a wall, *J. Aeronaut. Sci.* **24**, 468–469 (1957).
18. F. H. CLAUSER, The turbulent boundary layer, *Adv. Appl. Mech.* **IV**, 1–51 (1956).
19. R. L. SIMPSON, W. M. KAYS and R. J. MOFFAT, The turbulent boundary layer on a porous plate: an experimental study of the fluid dynamics with injection and suction, Dept. of Mech. Engng, Stanford University, Report No. HMT-2 (1967).
20. W. F. GIAUQUE and J. D. KEMP, The entropies of nitrogen tetroxide and nitrogen dioxide. The heat capacity from 15°K to the boiling point. The heat of vaporization and vapor pressure. The equilibria $N_2O_4 \leftrightharpoons 2NO_2 \leftrightharpoons 2NO + O_2$, *J. Chem. Phys.* **6**, 40–52 (1938).
21. M. BODENSTEIN and F. BÖES, Bildung und Zersetzung der höheren Stickoxyde, *Zeits. Phys. Chemie* **100**, 68–123 (1922).
22. R. A. SVHELA and R. S. BROKAW, Thermodynamic and transport properties of the $N_2O_4 \leftrightharpoons 2NO_2 \leftrightharpoons 2NO + O_2$ system, NASA TN D-3327 (1966).
23. W. A. ROSSER and H. WISE, Thermal decomposition of nitrogen dioxide, *J. Chem. Phys.* **24**, 493–494 (1956).
24. P. G. ASHMORE and M. G. BURNETT, Concurrent molecular and free radical mechanisms in the thermal decomposition of nitrogen dioxide, *Trans. Faraday Soc.* **58**, 253–261 (1962).
25. L. L. WILKSTROM and K. NOBE, Catalytic dissociation of nitrogen dioxide, *I/EC Proc. Des. Dev.* **4**, 191–195 (1965).
26. S. SOURIRAJAN and M. A. ACCOMAZZO, The application of the copper oxide alumina catalyst for air pollution control, *Can. J. Chem. Engng* **39**, 88–93 (1961).
27. E. T. DERGAZARIAN *et al.*, JANAF Thermochemical Tables, Thermal Laboratory, The Dow Chemical Co., Midland, Mich., December 1960 and supplements to date.
28. R. B. BIRD, W. E. STEWART and E. N. LIGHTFOOT, *Transport Phenomena*. Wiley, New York (1966).
29. C. R. WILKE, A viscosity equation for gas mixtures, *J. Chem. Phys.* **18**, 517–519 (1950).
30. E. A. MASON and S. C. SAXENA, Approximate formula for the thermal conductivity of gas mixtures, *Physics Fluids* **1**, 361–369 (1958).
31. Y. C. WU, A finite difference procedure for turbulent tube flows of an effective binary gas mixture with non-equilibrium chemical reactions and mass transfer, Ph.D. Dissertation, School of Engineering and Applied Science, University of California, Los Angeles (1970).
32. V. E. DENNY and R. B. LANDIS, An improved transformation of the Patankar–Spalding type for numerical solution of two-dimensional boundary layer flows, *Int. J. Heat Transfer* **14**, 1859–1862.
33. R. G. DEISSLER, Analysis of turbulent heat transfer and flow in the entrance regions of smooth passages, NACA TN 3016, (1953).
34. J. G. KNUDSEN and D. L. KATZ, *Fluid Dynamics and Heat Transfer*. McGraw-Hill, New York (1958).
35. A. F. MILLS, Experimental investigation of turbulent heat transfer in the entrance region of a circular conduit, *J. Mech. Engng Sci.* **4**, 63–77 (1962).
36. L. M. K. BOELTER, G. YOUNG and H. W. IVERSON, An investigation of aircraft heaters. XXVII—Distribution of heat transfer rate in the entrance section of a circular tube, NACA TN 1451 (1948).

ECOULEMENT TURBULENT D'UN MÉLANGE DE GAZ EN RÉACTION D'ÉQUILIBRE OU NON DANS UN TUBE AVEC TRANSFERT MASSIQUE PARIÉTAL

Résumé—Une méthode aux différences finies a été appliquée à des écoulements turbulents dans un tube pour des mélanges binaires de gaz idéaux en réaction chimique d'équilibre ou non et avec une injection de masse à la paroi du tube. On néglige la diffusion axiale des espèces, de la quantité de mouvement et de l'énergie thermique de façon à obtenir des équations paraboliques de conservation. La formulation de Van Driest pour la diffusivité par turbulence a été étendue pour inclure les effets des propriétés physiques variables et le transfert massique superficiel. On a développé les procédures de calcul pour introduire le modèle de diffusivité par turbulence à la fois dans les écoulements à couche limite interne et externe.

La méthode numérique globale a été appliquée à des écoulements d'air seul, de mélanges équilibrés de N_2O_4 et NO_2 et des mélanges hors d'équilibre ou non de NO_2, NO et O_2, avec injection de O_2 à travers la paroi du tube.

TURBULENTE STRÖMUNG VON GASGEMISCHEN MIT GLEICHGEWICHTS- UND NICHTGLEICHGEWICHTS-REAKTIONEN IN EINEM ROHR BEI STOFFAUSTAUSCH MIT DER OBERFLÄCHE

Zusammenfassung—Es wurde eine Differenzenmethode entwickelt zur Lösung von turbulenten Rohrströmungen von Zweistoff-Gasgemischen (ideales Gas) mit chemischen Gleichgewichts- oder Nichtgleichgewichts-Reaktionen und mit Massenzufuhr von der Rohrwand. Der axiale Diffusionsaustausch von Masse, Impuls und Wärme wurde vernachlässigt, um parabolische Gleichungen bei den Erhaltungssätzen zu bekommen. Der Ansatz von van Driest für den zusätzlichen Austauschkoeffizienten wurde erweitert, um auch die Auswirkungen variabler Stoffeigenschaften und des Massenaustauschs mit der Oberfläche zu erfassen. Es wurden Rechenprozeduren entworfen, die den Ansatz für den zusätzlichen Austauschkoeffizienten in die Berechnungen turbulenter Strömung bei Grenzschichten von durchströmten und umströmten Körpern einführen.

Die allgemeine numerische Methode wurde angewandt auf Strömungen von nichtreagierender Luft, Gleichgewichts-Mischungen von N_2O_4 und NO_2 und Mischungen im Nichtgleichgewicht von NO_2, NO und O_2, mit O_2-Zuführung durch die Rohrwand.

ТУРБУЛЕНТНОЕ ТЕЧЕНИЕ ГАЗОВЫХ СМЕСЕЙ ПРИ НАЛИЧИИ РАВНОВЕСНЫХ И НЕРАВНОВЕСНЫХ РЕАКЦИЙ В ТРУБЕ ПРИ НАЛИЧИИ МАССООБМЕНА НА ПОВЕРХНОСТИ

Аннотация—Разработан конечно-разностный метод для решения турбулентных потоков эффективно бинарных идеальных газовых смесей в трубе при наличии равновесных или неравновесных химических реакций, а также при наличии вдува через стенки трубы. При выводе основных параболических уравнений сохранения пренебрегается осевой диффузией массы, количеством движения и тепловой энергией. Обобщено выражение Ван-Дриста для коэффициента турбулентной диффузии с учётом переменных свойств и массообмена на поверхности. Разработана численная схема расчёта турбулентных потоков как для внутренних, так и для внешних пограничных слоев.

Общий численный метод используется для потоков нереагирующего воздуха, равновесных смесей N_2O_4 и NO_2, неравновесных смесей NO_2, NO и O_2 при вдуве O_2 через стенку трубы.